RESEARCH ARTICLE

TRIGGER: A Lightweight Universal Jamming Gripper for Aerial Grasping

PAUL KREMER [1,2], **HAMED RAHIMI NOHOOJI** [2], **(Member, IEEE)**,
JOSE LUIS SANCHEZ-LOPEZ [2], **(Member, IEEE), AND HOLGER VOOS** [1,2], **(Member, IEEE)**
[1] Faculty of Science, Technology and Medicine (FSTM), University of Luxembourg, 4365 Esch-sur-Alzette, Luxembourg
[2] Interdisciplinary Center for Security, Reliability and Trust (SnT), University of Luxembourg, 4364 Esch-sur-Alzette, Luxembourg

Corresponding author: Paul Kremer (p.kremer@uni.lu)

ABSTRACT This work introduces TRIGGER, the first ligh**T**weight unive**R**sal jamm**In**G **G**ripper for a**E**rial g**R**asping. TRIGGER is an omnidirectional, landing-capable aerial grasping system with resilience and robustness to collisions and inherent passive compliance. In particular, this work presents the design, fabrication, and experimental validation of a novel, intelligent, modular, universal jamming gripper specifically designed for aerial applications. Leveraging recent developments in particle jamming and soft granular materials, TRIGGER generates 15 N of holding force with only a relatively small activation force of 2.5 N. Experiments show the relationship between fill ratio and activation force and reveal that adding an additive to the membrane's silicone mixture improves the holding force by up to 52 %. Based on the experimental data, a simulation model for robotic simulators is introduced to facilitate future controller developments. To showcase the concept, TRIGGER is attached to a multicopter platform, performing a pick-and-place task under laboratory conditions. The aerial experiments are concluded by grasping a variety of shapes demonstrating the universal grasping capability.

INDEX TERMS Universal jamming gripper, aerial manipulation, soft gripper, soft robotics, grasping.

LICENSE

I. INTRODUCTION

During the last decade, Unmanned Aerial Vehicles (UAVs) attracted considerable research interest from the robotics community, especially when operating fully autonomously [1], [2]. In 2010 seminal work on fully functional UAVs for plant inspection for UK onshore oil refineries [3] was developed. Only a few years later, UAV technology had matured to a point where it could be utilized in several applications such as remote sensing and monitoring of forest fires [4], in agriculture [5], border monitoring [6], search and rescue [7], plant assets inspection [8],

transmission line inspection [9], building inspection [10], and non-physical human-drone interaction [11]. Despite the huge success UAVs had in sensing and monitoring applications, they fell short when it came to tasks that required physical interaction with their surroundings. Consequently, the field of aerial manipulation emerged, addressing those deficits by equipping UAVs with robotic manipulators [12] and claw-like grippers [13], [14]. In the last few years, aerial manipulation has considerably evolved, featuring numerous applications, including medical goods delivery [15], infrastructure monitoring and maintenance [16], [17], autonomous transportation and construction [18], agriculture [19], and forestry [20].

Several drone-grippers featuring a wide variety of grasping mechanisms were developed over the past years (see Table 1), e.g., pneumatic soft fingers [24], rigid jaw grippers [26], passive bi-stable grippers for micro UAVs [27], suction cups [21], magnets [22], and flexible limb grippers [32]. Some of these grippers are passively compliant, e.g., the soft finger-based grippers [24], while others are completely

TABLE 1. Comparison of robotic grippers developed for drones: archetype; the total mass m; maximum holding force F_h; F_h/m the holding force to mass ratio; actuation method; integrated sensors; passive compliance; omnidirectional (indifferent to grasping direction); capability to serve as landing gear; year of publication.

| Drone Gripper	Archetype	m (kg)	F_h (N)	F_h/m	Actuation Method	Sensors	Compliant	Omni-directional	Landing capable	Year
Self-sealing suction cup [21]	suction cup	0.72	12	1.7	pneumatic (pump)	pressure	-	✓	-	2016
Permanent Magnet Hand [22]	magnet	0.30	25.48	8.7	magnetic	contact	-	✓	-	2018
Actively Compliant Gripper [14]	arm+claw	0.30	0.57	0.2	servo (tendon)	/	✓	-	-	2018
Soft Grasper [23]	hand	0.58	10-20	3.5	pneumatic (cartridge)	/	✓	-	-	2018
Small Sleeved Gripper [24]	hand	0.38	52	14.0	pneumatic (cartridge)	/	✓	-	✓	2018
Ultra-fast Robot Hand [25]	hand	0.55	51	9.5	servo (tendon)	proximity	✓	-	-	2019
Mechatronic Jaw Gripper [26]	claw	N/A	2	N/A	servo (direct)	aperture	-	-	-	2020
Soft-Tentacle Gripper [16]	claw	N/A	32	N/A	servo (tendon)	force	✓	-	✓	2021
Micro Bistable Gripper [27]	claw	0.008	2.12	27.0	impact/motor	/	-	-	✓	2021
Hybrid Suction Cup [28]	suction cup	0.050	80	163.1	pneumatic (pump)	pressure	-	✓	✓	2021
Closed-Structure Gripper [29]	iris	0.27	5-15	5.7	motor (tendon)	/	✓	✓	✓	2021
RAPTOR [30]	claw	N/A	N/A	N/A	servo (direct)	/	✓	-	-	2022
HASEL Gripper [31]	hand	N/A	0.8	N/A	hydraulic/electrostatic	/	✓	-	-	2022
TRIGGER	UG	0.38	15	4.0	pneumatic (pump)	force, pressure	✓	✓	✓	2023

rigid, e.g., [22] and [26]. In practice, both approaches are viable, and the optimal choice of the gripper is ultimately application dependant [33]. As a rule of thumb, rigid grippers are less versatile since they are made for specific payloads (e.g., box-shape objects [26], or for specific materials [22]), heavier due to mechanical joints, but in turn, can provide a more secure grasp for the payloads they are optimized for. On the other hand, soft grippers can grasp a broad variety of payloads [24] by passively conforming to the grasped objects. Their soft structure allows them to soften the impact and thus reduce the contact forces that can potentially destabilize the drone. Furthermore, soft grippers are generally more tolerant towards position errors which are inevitable due to the ground effect [34]. These features make soft grippers very promising candidates for grasping in complex, unstructured environments [35]. There is however no free lunch, and the gain in versatility is often paid for by compromising in other areas, e.g., cycle time.

The prevailing soft gripper type in aerial manipulation is the soft-finger gripper actuated either pneumatically or via a tendon system, with their fingers arranged in a hand or claw configuration. They are often used to either grasp objects, or to attach the UAV to a location of interest (e.g., resting on a pipe for inspection). Especially pneumatic soft finger grippers suffer from being a substantial effort to manufacture and also from requiring high operating pressures in the range of $100\,kPa$ to $250\,kPa$ to generate substantial holding forces, while tendon actuated fingers are generally only semi-soft. Furthermore, the high air pressure required to drive the fingers is usually beyond what miniature air pumps are capable of and thus has to be provided by replaceable CO_2 cartridges. Their soft, rickety nature and the particularities of their grasping mode have also shown to be a challenging control and planning problem [36].

In [37], a very particular type of soft gripper was introduced, namely, the *Universal Jamming Gripper* (UG), which is a pneumatic gripper based on the jamming principle of certain granular materials. This UG, being in essence just a bag containing granular material, works via three distinct mechanisms and respective forces that are simultaneously involved in the grasping process, namely geometric interlocking F_G, suction F_S and friction F_R, which all come into play once the soft membrane of the gripper is pressed against the payload by a force called *activation force*. After jamming (hardening) of the granular material [38], the resulting *holding force* is then the sum of all components: $F_h = F_G + F_S + F_R$. The jamming typically involves creating a vacuum inside the membrane; however, other jamming principles exist, e.g., by magnetic fields [39], or hydraulic fluids [40]. As discussed in [41], UGs have virtually infinite degrees of freedom that do not need to be controlled explicitly, which gives them the characteristic of being able to grip objects of vastly different shapes thanks to the passively compliant membrane. Given their symmetric shape, they have no preferred in-plane (horizontal) grasping direction and are thus omnidirectional. UGs tolerate relatively large positional and angular (tilt) errors during the grasp [37], [42]. It is shown in [41] that off-center grasping with a positional error of up to $60\,\%$ of the membrane's radius does not degrade the gripper's grasping capability. The versatility and the relaxed requirements for positional and angular accuracy and, consequently, less stringent control requirements serve as the main motivation for developing the UG described herein. The structure of the UG is well suited to double as the drone's landing gear (contrary to the ubiquitous soft finger grippers). Furthermore, UGs provide rigid-like grasps by the jamming of the granular material.

Granular jamming is one of the fundamental mechanisms behind UGs. A range of materials exhibit jamming under compression, but the bulk properties of the hardened material can be vastly different as they depend on grain size, shape, and hardness. The properties of jamming materials in the context of grasping have been the subject of many studies, e.g., [43], [44], [45], and [46]. The authors of [46] concluded that the optimal granular material is ultimately application dependant. The membrane morphology was studied in [47], and it was
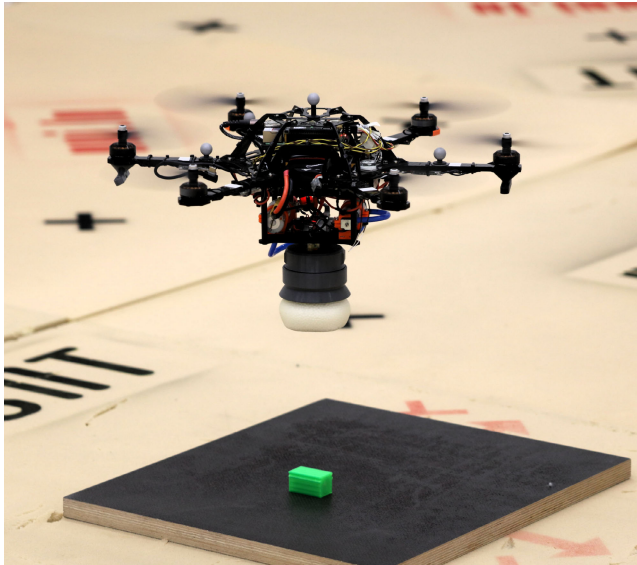
FIGURE 1. General aerial grasping concept. TRIGGER is attached to the UAV's cargo bay, similar to a claw-gripper. The UAV's landing gear has been removed as the gripper assures this functionality. The box (green) serves as the dummy payload.

identified that the widely used bag-style membrane is not necessarily optimal. Membrane patterning and programmed deformations can further improve the grasping performance for certain objects [48]. In [49] it was found that the membrane's material and the applied vacuum pressure impact the jammed membrane's overall stiffness.

By introducing TRIGGER (ligh**T**weight unive**R**sal jamm**In**G **G**ripper for a**E**rial g**R**asping) this is the first study that adapts the original concept of the *Universal Jamming Gripper* presented in [37] for aerial manipulation. The proposed design shares many advantages of available soft grippers in the field, e.g., [36] and [30], such as resilience and robustness to collisions and the inherent passive compliance, which decouples the UAV from the environment. However, the salient features of the proposed system lie in the intuitiveness of the design, in the simplicity of its omnidirectional grasping mechanism and in its ability to also serve as landing gear. Compared to soft finger grippers, the presented gripper features a grasping mode that we think is more practical for use in aerial manipulation and, although not without challenges of its own, reduces the complexity of the manipulation task with respect to planning and control.

The main contributions of this work are summarized as follows:

1) To the best of the authors' knowledge, this is the first work that conceptualizes, discusses and uses UGs in aerial manipulation. UGs can relax the aerial vehicle's dependency on the grasping direction and the required positional accuracy. Therefore, this work addresses open challenges regarding aerial grasping in complex environments [35].
2) This work presents a new design and implementation of a UG called TRIGGER, a lightweight and compact

gripper for aerial manipulation. By analyzing the relation between activation force and fill ratio, we designed TRIGGER to work with a much lower activation force than traditional UGs (e.g., [43], [50]), making it suitable for small to medium-sized aerial platforms. It is shown that the holding force can be increased substantially with the help of a silicone additive. We share the design and manufacturing process as well as the challenges and solutions encountered during the development of our gripper.

3) We present extensive experimental validation of our design in conjunction with our custom test jig. Based on the experimental data, we propose a simulation model of our UG. The effectiveness of TRIGGER is demonstrated by attaching it to a multicopter, performing a pick-and-place task, and repeated picking tasks for a variety of synthetic shapes, showcasing the gripper's universal grasping capability under laboratory conditions.

The rest of this work is organized as follows. Section II introduces the main design challenges and solutions associated with the design and manufacturing of TRIGGER. In Section III, TRIGGER is characterized followed by the presentation of the experimental results regarding the activation force and the impact of the silicone additive on the holding force. Based on the experimental data, a model of the developed gripper for robotic simulators is proposed in Section IV. Section V showcases TRIGGER in an aerial application. Section VI discusses the design and main findings. This work is summarized in Section VII.

II. CONCEPT AND SYSTEM ARCHITECTURE

In this section, we first introduce the general concept of our UG and the associated design challenges in the context of aerial manipulation. We then take an in-depth look at the electro-mechanical, pneumatic, and software components.

A. CONCEPT

Multirotor platforms come with many benefits but also with a set of limitations. The most relevant ones are their limited payload capability, the constrained volume for attachments, their underactuated nature, and the challenging dynamics coupling. The dynamics coupling is particularly important for aerial systems carrying manipulators [51], but it also poses a problem for simpler 'claw' setups where only the grasping element gets in contact with the environment. Elastic elements inserted in the construction of the grasping device efficiently reduce the dynamic coupling by softening the hard shocks associated with typical grasping operations. Those elastic elements are inherently present in UGs as represented by their soft membrane. UGs are thus an ideal fit, provided they can be constructed to fit the size, weight and power envelope of aerial platforms.

Our proof-of-concept aerial platform is a medium-sized (wheelbase of 430 mm), modified *AscTec Firefly* hexacopter with a maximum payload capacity of 1 kg. This airframe
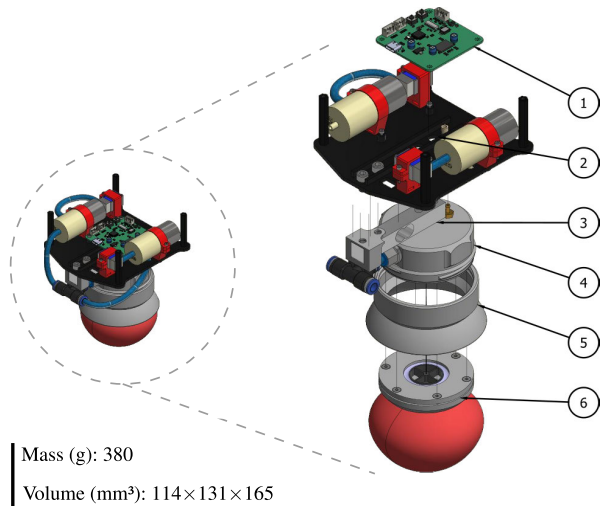
FIGURE 2. Complete assembly of the grasping system. ① custom controller board, ② base assembly with pneumatic system, ③ load cell, ④ gripper-floor, ⑤ wedge with thread, ⑥ membrane module.

conveniently features a cargo bay measuring 120 mm × 120 mm, which is used as the anchor point for TRIGGER. This particular mounting scheme with the gripper oriented towards the bottom is commonly called a 'claw'.

Compatibility with state-of-the-art autopilots (e.g., Pixhawk) is assured by either directly connecting the gripper to the autopilot via UART or by connecting it to the corresponding companion computer using USB. For ease of integration, our concept envisions being directly powered by the UAV's main 3S-4S battery, which eliminates the need for carrying an additional battery. Lightweight construction, modularity, and tight integration of the electronics, the sensors, and the software are the driving concepts of TRIGGER.

To make our work easily reproducible, accessible, and low-cost (below $100, without the manufacturing equipment), we limited our design to widely available and inexpensive manufacturing techniques, where a Fused Deposition Modeling (FDM) printer and a high-power single-stage vacuum pump represent the bulk of the cost. Furthermore, we designed our gripper around customary off-the-shelf parts.

The complete grasping system is detailed in Fig. 2. Its major subsystems are explained hereafter.

B. PNEUMATICS AND MECHANICS

The role of the pneumatic system is twofold: i) to pressurize the membrane and thus allow the contained granular material to flow easily within the free, air-filled volume; ii) to vaccumize the membrane and consequently jam (i.e., solidify) the granular material.

UGs can be realized in two distinct topologies, i.e., either as closed-loop or open-loop systems. In closed-loop systems, the fluid surrounding the granular material stays contained within the system. An example of such a system is the magnetorheological fluid-based UG shown in [39] for the

hydraulic UG presented in [40]. Generally, these systems have the main disadvantage that the fluid has to stay contained within the system (e.g., in tanks that add weight and cost) and that leakage must be considered as a critical failure mode. On the other hand, open-loop systems exchange their fluid with their environment. The operating fluid in that case is thus typically air, resp. water for underwater applications [52]. Those systems have the salient advantage that their fluid is abundantly present in their surroundings, which eliminates the storage needs and reduces the severity of leakage, e.g., due to membrane rupture. Open-loop systems are generally better suited for lightweight construction and require less engineering effort.

Therefore, the pneumatic system presented in this paper (Fig. 3) has an open-loop structure and uses air as its operating medium. It consists of two small, non-reversible diaphragm pumps (P1, P2) coupled to two pneumatic solenoid 2/1-way valves (V1, V2). The air pressure in the system is measured by the Microelectromechanical System (MEMS) pressure sensor P. This particular setup is very low cost and has a favorable mass distribution due to symmetry. By design, diaphragm pumps act as one-way check-valves, not restricting the airflow in their nominal direction, which therefore requires closing the valve associated with the antagonistic pump such that they can establish a pressure differential. This particular topology also permits to seal off the system. The membrane can thus remain pressurized (resp. in a state of vacuum) without powering the pumps, which saves energy.

We utilize two 12V, 7 W, SC3704PM diaphragm pumps rated for a pressure differential of 46 kPa at 2 L min^{-1}. The miniature 2/1 air valves are of type SCO520FVG. Our low-power pneumatic system typically consumes less than 10 W, contrary to other systems frequently featured in the literature, which are using heavy (more than 1 kg) stationary, high-power vacuum pumps in the 500 W range and reaching pressure differentials beyond 80 kPa [37], [44]. Note that our lower-power system naturally comes with longer cycle times and a lower maximum pressure differential (we measured approximately 28 kPa), 3 times lower than conventional solutions. The lower pressure differential normally impacts the jammed stiffness of the granular material as shown in [49], which negatively impacts the holding strength. However, as shown in Section III-C, we found that a simple modification to the silicone mixture can greatly enhance the gripping strength of the UG, offsetting the effects of the weaker vacuum.

Concerning the mechanical structure, our modular design approach is shown in Fig. 2. It consists of three larger subassemblies, namely i) the base, containing the controller board ①, the pumps and the valves ②. ii) the gripper-floor ③ to ⑤, forming the interface between the pneumatic system and the detachable membrane module, iii) the membrane module, which firmly holds onto the filled, custom silicone membrane. It contains a paper filter that seals off the filler material from the environment while permitting air to circulate freely. A mechanical support structure prevents it from
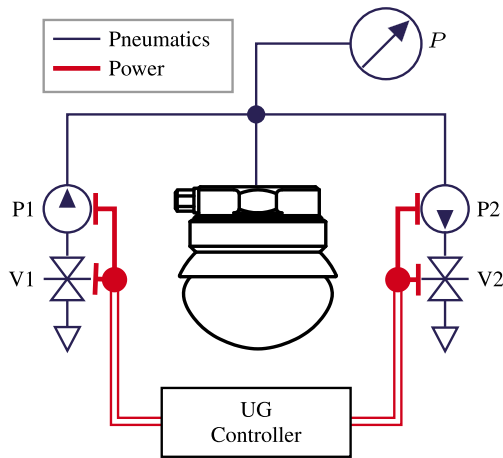
FIGURE 3. Pneumatic system. The jamming gripper is fed by two pumps. Pump P1 inflates the balloon and fluidizes its content. Pump P2 creates a vacuum strong enough to jam the particles inside the balloon. The solenoid valves V1, V2 are required to prevent air from leaking through the inactive pumps. All pneumatic components are actuated based on the control inputs from the main controller.
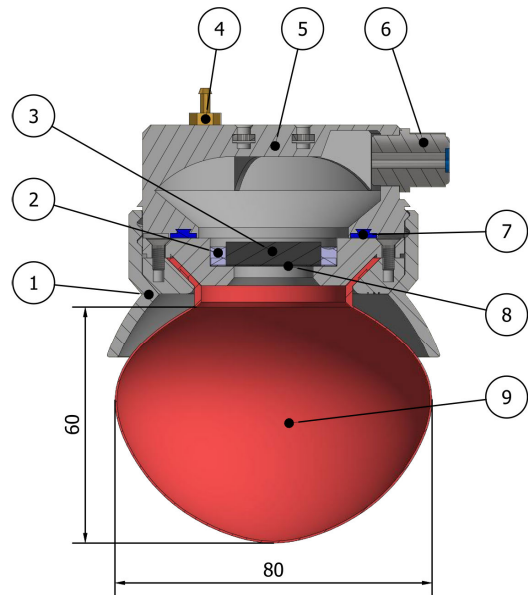

FIGURE 4. Section view of the main gripping module (membrane module attached to the gripper-floor). (1) wedge with integrated thread, (2) hot-glue seal, (3) mechanical filter support, (4) pressure gauge fitting, (5) upper shell, (6) main air inlet/outlet, (7) cast-in-place silicone gasket, (8) paper filter, (9) membrane filled with granular filler material.

tearing under load. The membrane module (6), detailed in Fig. 4, is firmly pressed against the cast-in-place silicone seal on the gripper-floor by screwing the wedge onto the external printed thread to create an air-tight seal.

This modular concept has three main advantages: *first*, it enables quick iteration on membrane module designs; *second*, it allows to quickly and effortlessly swap between different membrane modules during the tests; *third*, it enables the platform to be compatible with different types of grippers, given that there are some geometries that cannot be picked up by a UG (e.g., large flat surfaces), which require highly specialized grippers such as vacuum cups.

Our UG is designed to be mounted like a 'claw' on a multirotor; therefore, it does double duty, i.e., it operates as a gripper but also serves as the landing gear. As such, it is dimensioned to withstand the total weight and impact of a landing UAV, which comes with several advantages that we discuss in Section VI.

C. MATERIAL SELECTION & FABRICATION

The membrane is made from the silicone rubber *Trollfactory Type 23*, shore hardness 10 A with 600 % elongation at break. Selecting a very soft rubber comes with two main advantages: *first*, it allows wider tolerances on the membrane's thickness as small deviations no longer have a significant impact on the overall stiffness; *second*, it maximizes the contact area between the membrane and the payload and therefore the quality of the grasp is increased. Furthermore, this particular silicone can be mixed with a silicon additive called *deadener* (also sometimes referred to as *slacker*), which gives the silicone more skin-like physical properties. This further increases the softness of the material and, more importantly, makes it sticky. The intensity of those effects is controlled by the relative amount of additive added to the mixture.

Based on our previous experience with silicone [53], a silicone casting process was used to create the membrane. A three-part mold (i.e., left and right shell, plus core) was printed from PET-G using common FDM printing. The approach is similar to [40]; however, due to the very thin 0.6 mm membrane and the high viscosity of the silicone rubber (14 Pa s), the process had to be adapted to avoid trapping air inside the mold and thus creating voids in the thin membrane. Instead of pouring the silicone into the mold, it has proven advantageous to inject the silicone directly through the core using a syringe as depicted in Fig. 5. This technique enables very thin-walled castings (assuming proper alignment of the shells) as it allows the silicone mixture to spread evenly with a fairly low risk of introducing air bubbles in the process. The usual precautions were taken when working with silicone, such as properly degassing the silicone after mixing. The final membrane has a nominal diameter of 80 mm, a thickness of 0.6 mm, a height of 60 mm, an encompassing volume of 0.2 L and a total mass of only 18 g (without filler).

The choice of the filler material has a substantial impact on the grasping performance of jamming grippers, as concluded in [46]. Furthermore, the authors indicated that it has to be considered as an application dependant design variable. Aiming for a lightweight design, in addition to raw performance, the density of the filler material also plays a key role. Expanded Polystyrene (EPS) beads (various sizes ranging from 1 mm to 4 mm) strikes a good compromise between the two, as shown in [44] and [46]. With only 17 g L^{-1} EPS is considerably lighter than other commonly used filler
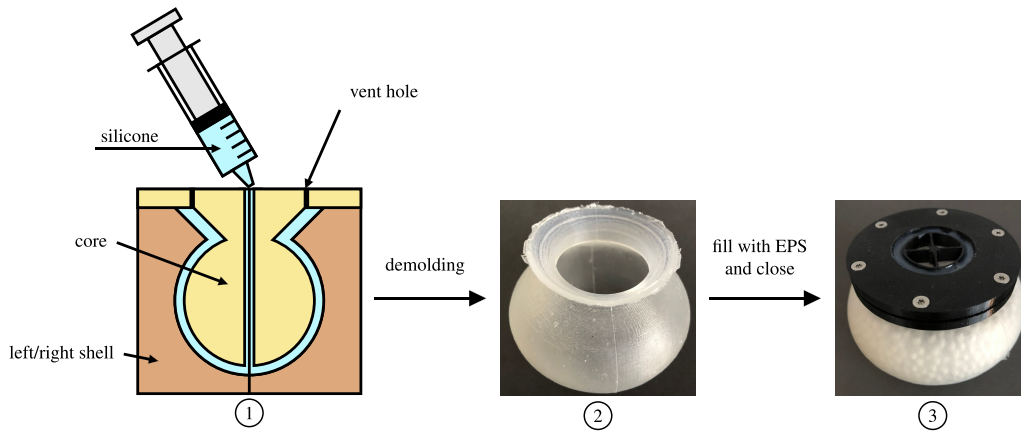
FIGURE 5. Fabrication process of the membrane. ① The degassed silicone mixture is injected with a syringe through the mold's core. The air inside the mold escapes through the vent holes at the top. Precise alignment between the shells is critical as the membrane is only 0.6 mm thick. ② The obtained membrane after demolding. ③ The membrane is filled with EPS and closed with a mechanical assembly that contains the filter. The resulting gripper module is thus fast and easy to swap out in case of damage.

TABLE 2. Comparison of filler materials. EPS has by far the lowest density.

Material	Density (g L^{-1})	Particle Size (mm)
EPS	17	1-4
Coffee	308	0.2-2
Polymer	940	0.1-0.2
Glass	2500	0.2-0.4

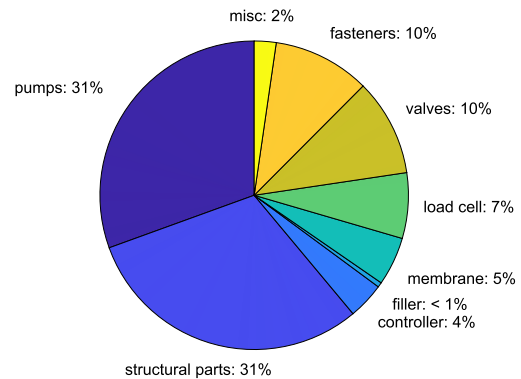**FIGURE 6.** Mass breakdown of the total mass of the assembly (380 g). The pumps and the structural plastic parts form the bulk of the mass.

materials, e.g., ground coffee with a density of 308 g L^{-1} or glass beads with 2500 g L^{-1}, see Table 2. A total of 2.2 g of EPS (0.13 L) was added to the membrane (unless otherwise indicated), which corresponds to a fill ratio of 66 %.

The printed structural parts are made from PET-G. Compared to PLA it has higher impact resistance, lower density and does not creep under sustained load. The structural parts would not benefit from high-end polymers such as PA6-CF or PEEK as there are no special requirements concerning the stiffness or heat resistance that could motivate such a choice. The resulting parts have proven to be sufficiently airtight using optimal print settings. At the mating points of two structural parts (i.e., ⑤ and ⑧ in Fig. 4), a cast-in-place silicone gasket assures an air-tight seal between the two parts.

The total mass of the assembly (380 g) is distributed among the different components as shown in Fig. 6. The pneumatic system represents the bulk of the mass (160 g), followed by the structural plastic parts (115 g) and the fasteners (35 g), fittings and tubing (less than 8 g).

D. ELECTRONICS AND FIRMWARE

The system depicted in the block diagram in Fig. 7 is implemented on a single, completely custom 47 mm × 47 mm controller board which is shown in Fig. 2. It is designed to work and integrate easily with common UAV hardware. As such, it can be powered directly from the main power bus of the drone. Furthermore, it features USB and UART serial

ports for communication with an autopilot or an off-board computer.

At the heart of the controller is an ultra-low power STM32L1 microcontroller that does the logic processing, collection/processing of the sensor data, the communication with the off-board peripherals, and the control of the quad-channel motor driver that powers the pneumatic hardware.

Due to the low power requirements of the controller (less than 50 mA at 12 V) we have favored linear DC/DC regulators over switching converters for the 5 V and 3.3 V rails as the latter greatly increase the design complexity and cost. The output stage (valves and pumps) is directly powered by the main power bus. Current chopping motor drivers ensure that each actuator operates at its nominal operating point regardless of the bus voltage.

The load cell and the onboard air pressure sensor provide the required data for the system to monitor itself and to work autonomously. The processed sensor readings are exposed via serial to enable more advanced applications. Such applications include activation force tracking, the possibility of
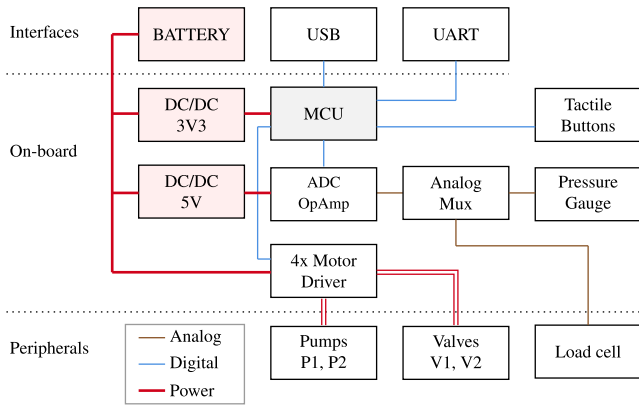
FIGURE 7. Sensors and control topology. The system features a quad-channel current-chopping motor driver for the pumps P1, P2, and valves V1, V2. The sensors (pressure gauge and load cell) are interfaced through a multiplexer into a differential operational amplifier + ADC. Communication with the main microcontroller is assured via USB or UART. The power rails are generated from the battery using cascading linear voltage regulators.

Algorithm 1 FreeRTOS, Sensor Acquisition and Actuation

procedure task 1: sensors and actuation
    let k_{gr} be the current gripper state
    let $S(k_{gr})$ be the automaton in Fig. 23
    let f_1, f_2 be lowpass FIR filters
    loop
        collect push button states $\mathbf{u_{bt}}$
        fetch raw sensor data P^*, F_m^*
        process sensor data $P \leftarrow f_1(P^*), F_m \leftarrow f_2(F_m^*)$
        create state vector $\mathbf{q} \leftarrow (t, k_{gr}, P, F_m)$
        process automaton $\mathbf{u_a} \leftarrow S(\mathbf{q}, \mathbf{u}))$
        apply $\mathbf{u_a}$ to actuators
    end loop
end procedure
procedure task 2: communication
    loop
        outbound communication, send $\mathbf{q}$
        inbound communication, receive $\mathbf{u_{usr}}$
        create command vector $\mathbf{u} \leftarrow (\mathbf{u_{usr}}, \mathbf{u_{bt}})$
    end loop
end procedure

FIGURE 8. TRIGGER grasping a variety of objects, showing its universal grasping ability. ① Empty aluminium bottle, ② cardboard box, ③ semi-soft ball, ④ filled glass flask hold from the small top cover, ⑤ walnut, ⑥ filled glass flask held from the smooth, slippery side.

---

feeding back the weight of the grasped payload to the controller as a known disturbance, and the detection of a successful or unsuccessful grasp after takeoff based on the load cell readings. We refer to the measured force F_m in gram-force 'gf' and the measured pressure as P in 'kPa'. This enables applications such as controlling the activation force and also empowers the internal logic to control the pressure inside the membrane and to prevent conditions such as membrane rupture due to over-pressure and to assure a consistent air pressure while approaching the payload.

We define two pressure thresholds, namely $P_{min} = -21$ kPa, the lower trigger point, and $P_{max} = 0.5$ kPa the upper trigger point. Those trigger points are used to switch reliably between the 'closed' and 'opened' states of the gripper. In particular, $P \geq P_{max}$ signals that the membrane is full and any additional air would stretch the membrane (consequently increasing the internal pressure). $P \leq P_{min}$ signals that a vacuum is established and thus the gripper is considered 'closed'.

The firmware on the MCU is making use of *FreeRTOS*, running two tasks using preemptive multitasking as shown in Algorithm 1. Task 1 handles sensors and actuation, and task 2 handles serial communication. Inter-task communication takes place over thread-safe FIFO queues. For the underlying state machine (automaton), we direct the reader to the Appendix.
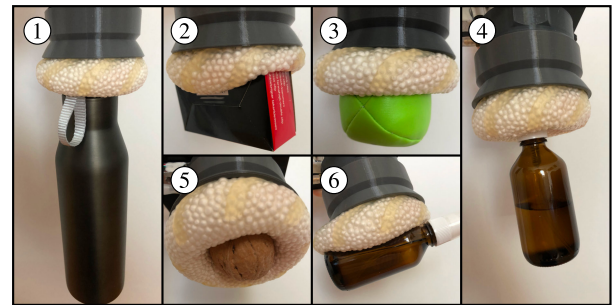
E. GRASPING PROCEDURE

Although usage of our UG by hand is straightforward and allows grasping of a variety of shapes and materials (see Fig. 8), a defined grasping procedure is required for our aerial platform such that successful grasps can be achieved without relying on human intuition. Typically this procedure consists of four main steps (Fig. 9, ① to ④):

① The grasp starts by pushing the fluidized gripper against the payload. Doing so elastically deforms the membrane and the filler material flows freely, distributing itself around the payload. At this point, valves V1 and V2 are still closed such that the free volume remains unchanged. The evacuation phase is then triggered once the measured force reaches the desired activation force, i.e., $F_m \geq F_a$.

② Evacuating the air out of the membrane takes a couple of seconds (governed by the flow rate of the pumps). During that period, the membrane shrinks, and the contact force drops in response to that unless the gripper is further moved toward the payload. In the context of low activation forces, it is essential to keep good contact with the payload. Failure to do so will lead to a poor or unsuccessful grasp as the filler hardens without properly surrounding the payload. We thus track the nominal activation force during this interval. Other publications

in this field usually avoid this step by pushing the gripper with a very high force into the payload, e.g., with 17 N as seen in [43], which is, however, not possible with most small to medium aerial systems. The pressure inside the membrane starts dropping once it reaches its minimal volume (see ⓐ). At that point, the granular material is compacted. Furthermore, the drop in pressure follows an exponential law as the remaining air molecules become harder to extract.

③ Once the membrane's internal pressure satisfies $P \leq P_{min}$ (vacuum, ⓑ), the grasping procedure is considered completed. The gripper is then retracted from the payload (here, at a constant velocity). Since the payload is fixated on the support and cannot be lifted, a negative force is measured. The peak of the force corresponds to the maximum holding force F_h. In practice, with the gripper mounted on a UAV, instead of the holding force, the actual weight of the lifted payload would be measured, which can be fed back into the autopilot.

④ Releasing the payload (i.e., opening resp. resetting the gripper) is achieved by pumping air into the membrane ⓒ until $P \geq P_{max}$ is reached at ⓓ, then closing valves V1 and V2. The gripper is now ready to grasp the next object.

The activation force F_a is an essential quantity for a successful grasping operation. An insufficient activation force causes the grasping operation to fail. On the other hand, choosing F_a too high may destabilize the aerial platform and also cause damage to the force sensor and membrane. Therefore, the optimal activation force has to be chosen sufficiently high not to sacrifice performance but also as low as possible to minimize the impact on the aerial platform.

III. EXPERIMENTS
In the following section, we introduce our experimental setup as well as the experiments to, *first*, determine the optimal minimal activation force for the grasping procedure, and *second*, to access the influence of the silicone additive *deadener* on the grasping performance.

We also use this experimental setup to collect data regarding the stiffness of the UG in various states with the goal to create a simple simulation model resp. contact model for common robotics simulators (Section IV).
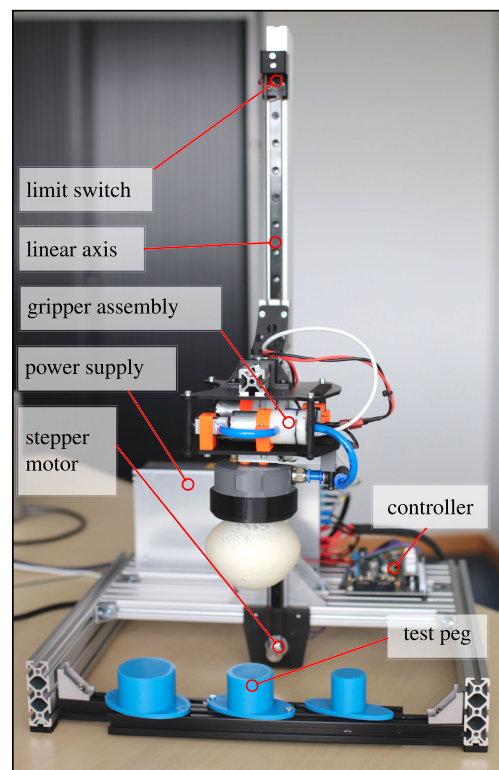
A. EXPERIMENTAL SETUP
Our experimental jig used for benchmarking is featured in Fig. 10. It consists of a 12 V supply and a single belt-driven linear rail (capable of fast movements) moving the entire gripper assembly fixated to the horizontal beam. The stepper motor is powered and controlled by an off-the-shelf *3D printer board*. The jig does not feature any sensors since they are already integrated into the gripper itself.

Velocity commands u_{feed} as well as position commands (G-codes) are accepted by our custom firmware on the jig's controller. The current position and velocity are sent back to
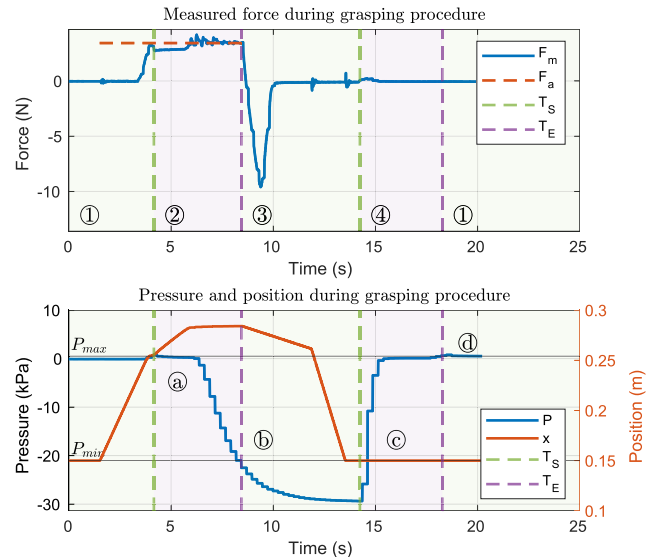
FIGURE 9. Grasping procedure. ① Approach, ② evacuation phase where the air is pumped out of the membrane, ③ retraction phase where the peek marks the maximum holding force, ④ reset of the gripper by pumping air into the membrane, ⓐ the pressure starts dropping once the volume reaches the minimum, ⓑ end of closing procedure triggered by $P \leq P_{min}$, ⓒ pressure rises as air is pumped in, ⓓ end of opening procedure triggered by $P \geq P_{max}$. T_S and T_E mark the start and the end of the state transition between open and close and vice-versa.

FIGURE 10. Experimental jig. The UG is attached to a belt-driven linear rail, moving the gripper assembly into contact with the test peg (blue). The test peg is a simple cylindrical object with no features allowing geometric interlocking.

the host computer for the purpose of logging. Likewise, the gripper's controller sends back its current state and sensor

data (force, pressure, and input voltage) while also accepting state transition commands (open/close).

Cylindrical test pegs (blue) represent the dummy payloads. They are fixated at the bottom of the linear axis, such that they cannot be lifted. The center of the pegs is aligned with the center of the membrane. They have no features that would allow for geometric interlocking. As such, the results concerning F_h can be seen as a worst-case scenario.

All of our experiments require tracking of a nominal activation force. As such, given a nominal force F_d and the measured force F_m, we want to drive the error e_f close to zero:

$$e_f = F_d - F_m. \tag{1}$$

The input u_{feed} is the commanded linear velocity of the sled. The system itself acts as an integrator since F_m is a function of the position, and as such e_f is guaranteed to be driven close to zero by the simple proportional control law

$$u_{feed} = K_p e_f, \tag{2}$$

where K_p is a positive constant.

B. MINIMUM ACTIVATION FORCE

The activation force is a crucial factor for a successful grasp. However, in the context of aerial manipulation, where the base of the gripper is floating, this becomes an even more important factor as any external forces have the potential to cause stability issues. We would like to point out the following key aspects:

- An aerial platform is severely limited in the amount of force it can apply to its environment before hitting its stability margins.
- Under some circumstances, e.g., when the target is poorly supported, it is impossible to apply a substantial activation force.
- The need for a (large) activation force can thus be seen as a net disadvantage of these types of grippers. Reducing it is therefore considered beneficial.

Recent research reported that there is a monotonic relation between the activation force and the resulting holding force [43]. An older study found that after reaching a certain threshold, the holding force stays constant [50]. Our results confirm the findings of both studies and indicate that this threshold depends on the fill ratio of the membrane.

In this study, we focus on small activation forces $F_a < 650$ gf as they are the most useful for aerial grasping. We thus conduct six test series with nominal activation forces ranging from 150 gf to 650 gf for fill ratios of 66% and 90%. Each test series follows the grasping procedure described in Section II-E and is repeated eight times using the $\varnothing 40$ mm peg. For this and all subsequent experiments, we have chosen $K_p = 6$ as a compromise to achieve reasonable force tracking while the membrane is still soft and to reduce overshoots when the membrane hardens at the end of the evacuation phase.
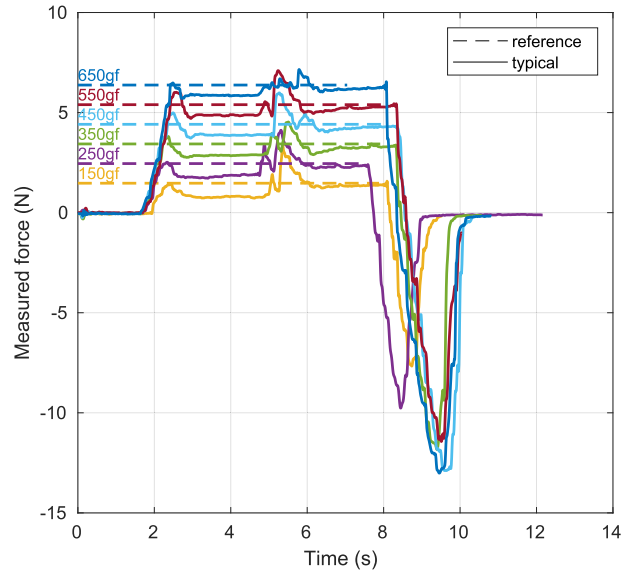

FIGURE 11. Activation and holding force for various nominal activation forces from 150 gf to 650 gf with a 66% fill ratio and no deadner. The nominal activation force is tracked during the whole evacuation phase (2s to 8s). The maximum holding force is then measured during the retraction phase (8s to 10s), where it shows up as the peak negative force.

The results of this study are shown in Figs. 11 to 13. The data shows that TRIGGER can reach a maximum holding force $F_{h,max}$ of about 10 N for the test peg with $D = \varnothing 40$ mm and without geometric interlocking. The evacuation period typically takes $T_{SE} = T_E - T_S = 4.3$ s (Fig. 9). Furthermore, there is a clear relationship between the fill ratio and the minimal activation forces required to reach the maximal holding force, as illustrated in Figs. 12 and 13. Lower fill ratios generally reduce the required minimum activation force. The gripper with the membrane having the lower fill ratio of 66% reaches $F_{h,max}$ with an activation force of only 250 gf (see Fig. 12). Increasing the activation force beyond that threshold does not significantly increase the resulting holding force. In case of the higher infill ratio of 90%, 650 gf are required to get the same holding force (see Fig. 13). Higher fill ratios naturally come with a smaller free volume, i.e., the volume in which the grains can move freely. In turn, the mobility of filler particles is impaired, which then requires a higher effort to redistribute the filler within the membrane during contact. This manifests in a monotonic relationship between the activation force and the holding force. Therefore the minimum activation force increases with the fill ratio.

We thus conclude that an activation force $F_a \geq 250$ gf is adequate for successful grasping without compromising the holding capability of the gripper. We consider this low enough to work on a wide range of UAVs without significantly impacting the stability of the aerial system. Furthermore, we conclude that lower fill ratios (in the 60% range) are preferable since they require lower activation forces.

C. DEADENER (ADDITIVE)

Deadener (also called *slacker*) is an additive that is added to the silicone during the mixing process. It alters the physical
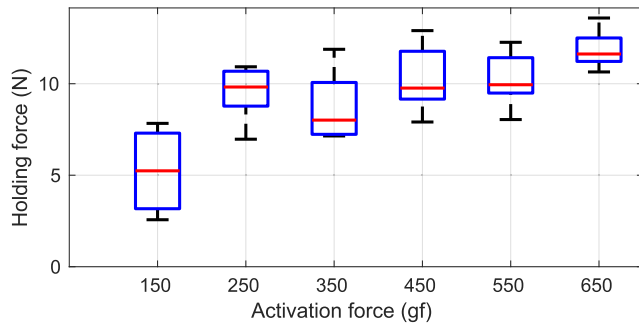
FIGURE 12. Holding force in relation to the nominal activation force, with a fill ratio of 66% and no deadener. The holding force stays constant after reaching the threshold of 250 gf.
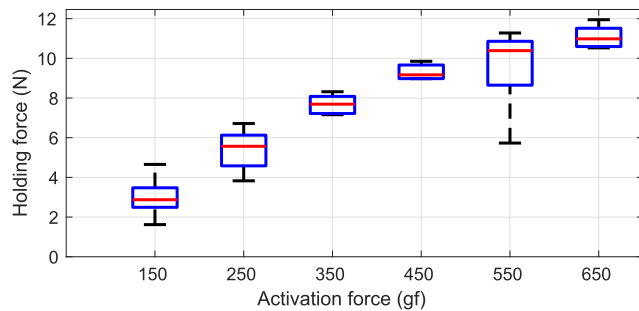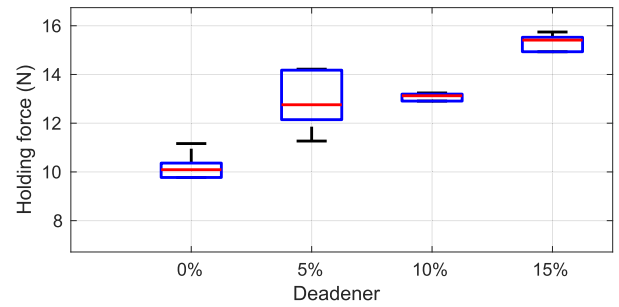

FIGURE 13. Holding force in relation to the nominal activation force, with a higher fill ratio of 90% and no deadener. The holding force increases monotonically with the activation force.

FIGURE 14. Holding forces for various percentages of deadener added to the silicone mixture of a membrane with 66% fill ratio. Increasing the amount of deadener makes the membrane softer and stickier, increasing the holding force. A nominal holding force of $F_a = 350\,gf$ was applied to all samples.

properties of the cured silicone by increasing its softness and stickiness.

Herein, we measured the effect of adding 0 % to 15 % of deadener (by weight) to the mixture. At around 15 % deadener, the membrane reached a consistency similar to chewing gum. Further increasing the percentage was thus deemed impractical.

For the test series, we created four membranes with 0 %, 5 %, 10 % and 15 % deadener (66 % fill ratio each). We repeated our holding force test 6 times for each of the membranes, with an activation force of 350 gf, on a ⌀40 mm test peg. The results are shown in Fig. 14. Starting with no deadener, we reach the expected holding force of around 10.1 N. A median of 12.8 N and 13.1 N was measured for 5 % and 10 % deadener, respectively. Further increasing it to 15 %, resulting in a median holding force of 15.4 N, a significant increase of 52 % compared to no deadener.

The increase in performance can be explained as follows. On one hand, the additive turns the membrane slightly tacky, thus increasing the friction coefficient between the membrane and the test peg. On the other hand, due to the increased softness, the membrane's ability to conform to the test peg's shape is improved, resulting in a larger contact surface. Both of them cause the contribution of the friction F_R to increase, which results in a greater F_h. It should be noted that the stickiness is a temporary effect and dwindles over time as the silicone ages and dust and dirt accumulate on the membrane's

surface. The lifespan assessment of the membrane is beyond the scope of this study and is thus left for future work. For a lasting effect, a clean environment is currently required. Alternatively, a periodic replacement/renewal of the membrane module (which is fully supported by our design, see Fig. 2) should be considered.

The adhesion does not interfere with the release of the objects. As the membrane is filled and restored to its fluidized state, any objects sticking to it are released due to its spherical geometry and the resulting reduction in the contact surface.

IV. MODELING

In the context of aerial manipulation, the UG exhibits challenging dynamic behavior as it transitions from a soft state to a jammed (almost rigid) state. This section proposes a homologous, uniaxial model of TRIGGER for use in robotic simulators, based on observations and measurements obtained from the experiments using the 15 % deadener and 66 % fill ratio membrane.

The model will faithfully represent the following main aspects of the UG:

1) the normalized free volume β represented as a first-order system, which models the transition between the membrane's open/closed states.
2) changes in β cause the membrane to shrink, resp., expand. Uniaxially, this effect is described by the free length x_a.
3) the contact force contribution of the air-filled membrane represented by the compression spring k_{air} as a function of the payload diameter D and the normalized free volume β.
4) the contact force contribution due to the lumped elasticity represented by the compression spring k_{lmp}, which takes into account the complete assembly with the gripper being jammed.

It is assumed that the membrane does not touch the ground during the grasping phase, which is the case for any reasonably sized payload.

We propose the contact model shown in Fig. 15, consisting of the two non-linear compression springs k_{lmp} and k_{air},
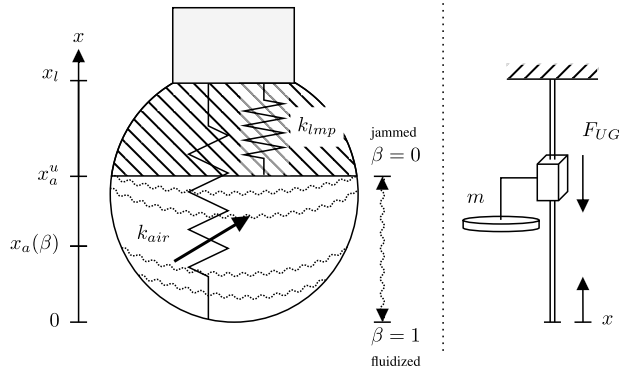
FIGURE 15. The UG membrane is separated into two components: the air-filled elastic membrane and the rest of the system. Both components can be seen as compression springs k_{air} and k_{lmp} in a parallel configuration (left). The simulated system consists of a disk (body) with a mass m attached to a prismatic joint with finite travel subjected to the combined elastic force F_{UG} (right).
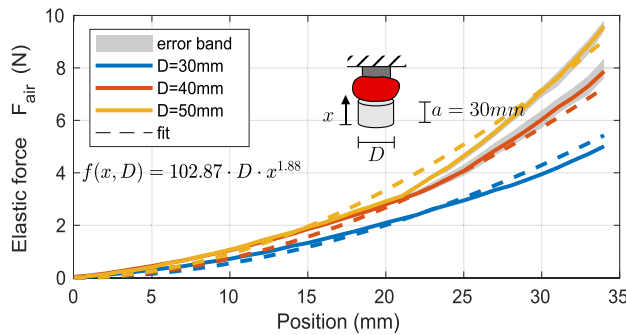
FIGURE 16. Elastic force F_{air} of the inflated membrane during contact with different sized test pegs from 30mm to 50mm. Larger effective areas generate a higher elastic force.

where the latter is of variable stiffness, i.e., dependant on the size of the targeted object. The spring k_{lmp} represents the lumped stiffness of the jammed filler material and the structural parts of the assembly. The spring k_{air} represents the compression of the air-filled membrane during contact. Its stiffness is tied to many parameters, such as the effective contact area, the non-linear elastic behavior of the membrane, internal pressure, filled volume, and other factors of which most cannot be measured. Its dynamic behavior is, to some extent, akin to an air spring, e.g., [54]. However, such a precise model is very hard to identify and has no practical benefits in this context.

We employed non-linear regression analysis to identify the relation between the depth of entrance x, the payload/peg diameter $D \in (0, 60]$ (in mm) and the resulting elastic force F_{air} as follows (Fig. 16)

$$F_{air}(x, D) = a_1 D x^{a_2}$$
$$= 102.87 \cdot D x^{1.88}. \quad (3)$$

Similarly, we identified the lumped elastic force of the system to be (Fig. 17)

$$F_{lmp}(x) = a_3 x^{a_4}$$
$$= 25119.75 \cdot x^{1.29}. \quad (4)$$
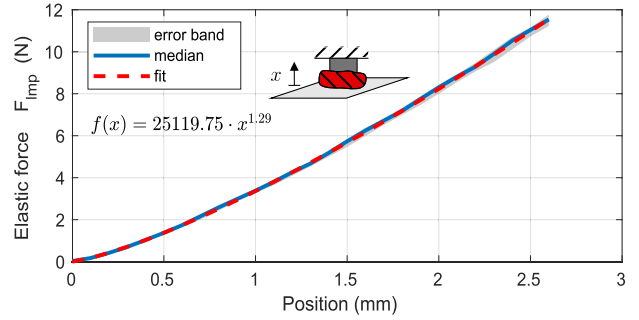
FIGURE 17. Lumped elastic force F_{lmp} of the jammed membrane-gripper system during contact with the test peg. The diameter of the test peg does not affect the results since the shape of the membrane does not change.

The combined elastic force F_{ug} is then obtained by

$$F_{ug} = F_{air}\left(H\left(x\right), D\right) + F_{lmp}\left(H\left(x - x_a\right)\right), \quad (5)$$

where

$$H(y) = \begin{cases} 0 & \text{if } y < 0, \\ y & \text{if } y > 0, \end{cases} \quad (6)$$

accounts for the fact that the springs act in compression only. The free length $x_a \in \left[0, x_a^u\right]$ depends on β and is modeled as the linear mapping

$$x_a = x_a^u \cdot \beta, \quad (7)$$

where the upper bound x_a^u is defined by the minimal volume occupied by the filler material in the jammed state. The constant $x_a^u = 40.8$ mm was determined experimentally and marks the position at which the jammed membrane first makes contact with the test peg.

The normalized free volume $\beta \in [0, 1]$ can be thought of as the volume fraction

$$\beta(t) = \frac{v(t) - v_F}{v_M - v_F}, \quad (8)$$

where v_F is the volume occupied by the filler material, and v_M is the volume encompassed by the unstretched, air-filled membrane. The membrane's shape defines the constants v_M and v_F. The time-variable air volume $v(t) \in [v_F, v_M]$ is controlled by the pneumatic system and is not measurable.

After the initial, unrestricted, constant flow pump down of the free air volume (i.e., $v(t)$ approaching v_F), the filler material starts opposing to further changes in volume. Consequently, the pressure differential increases (ideal gas law), and the flow rate drops. At that point, the topology of the pneumatic system is similar to a vacuum chamber, where the pump down is known to follow an exponential law. This is also confirmed by the pressure measurements shown in Fig. 9 (starting from $t = 6.4$ s). The volume $v(t)$ thus follows an exponential law motivated by the initial quasi-constant flow that approaches zero as the vacuum pump reaches its rated ultimate pressure.

Since $\beta(t)$ is just a normalized representation of $v(t)$ it exhibits the same first-order dynamics, which are defined in
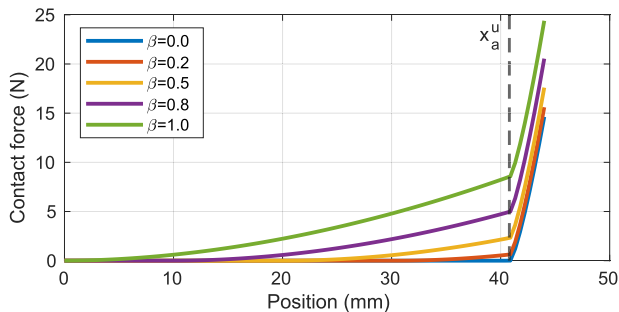
FIGURE 18. Contact force model for $D = 40mm$ with different membrane states from $\beta = 0$ (jammed) to $\beta = 1$ (completely filled with air). The lumped stiffness dominates starting from $x_a^u = 40.8mm$.

s-domain as

$$\beta(s) = \frac{R(s)}{1 + sT}, \qquad (9)$$

where $R(s)$ is a unit step (either 0 or 1, depending on the desired state transition), s is the Laplace variable, and T is the time constant of the system that can be approximated as $T = 63\% \cdot T_{SE}$ from the jamming transition shown in Fig. 9. Based on the value of β, it can be distinguished between three discrete states:

$$k_{gr}(\beta) = \begin{cases} \text{closed/jammed} & \text{if } \beta \leq 1\% \\ \text{opened/fluidized} & \text{if } \beta \geq 99\% \\ \text{in transition} & \text{otherwise} \end{cases} \qquad (10)$$

The contact force model (5) is visualized in Fig. 18 in function of x and β. It can be seen that the system becomes stiff as β approaches zero.

The contact model is the key component in creating a digital UG for use in a robotics simulator such as *Gazebo*. We propose modeling the UG as a disk with a diameter of 80 mm and a mass of $m = 20$ g (weight of filler plus membrane). That disk is attached to a prismatic joint that simulates the shrinkage of the membrane as a function of β, the intrusion of the payload into the membrane, and is subjected to a force F_{UG} governed by the contact force model (5). The travel limits of the joint are defined to be in the range of $[0, x_l]$, where $x_l = 60$ mm is the height of the membrane (see Fig. 15, right). The UG's internal state β is governed by the system model (9).

As for the grasping part, we suggest considering a grasp as successful as long as an activation force greater than 250 gf is maintained with the payload during the entire evacuation phase. A successful grasp should then establish a rigid connection between the gripper and the payload motivated by the jamming (hardening) of the filler material. That connection should be removed if $F_m \geq F_h$ or as a result of the state transition k_{gr} from 'closed/jammed' to 'in transition'.

Another application of the contact model (5) could be the estimation of payload size with the help of characteristic curves of the elastic forces identified during the initial contact, as shown in Fig. 16. However, this requires precise
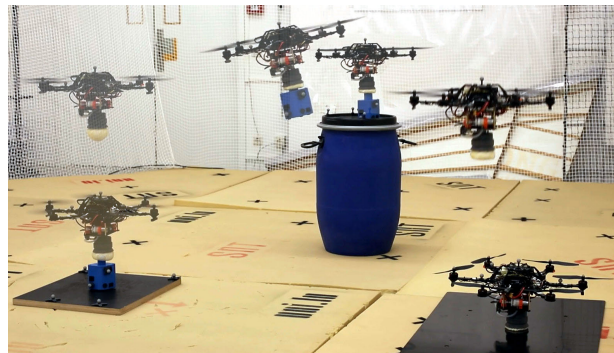
FIGURE 19. Aerial pick & place application. The UAV resting on the gripper takes off and picks up the payload in blue. The grasped payload is then placed on top of the barrel. Afterward, the UAV returns to the starting area for landing.

position measurements, which may not be available in real-world conditions.

V. AERIAL EXPERIMENTS

In this section, a pick-and-place task and a series of tests are presented to assess the grasp success rate of the overall aerial platform for various synthetic shapes.

### A. EXPERIMENTAL SETUP & METHODOLOGY

Our proof-of-concept platform based on the frame of an AscTec Firefly features a Raspberry Pi 4 with a Pixhawk autopilot. TRIGGER is mounted to the bottom of the hexacopter in a 'claw' configuration The Raspberry Pi is connected to the gripper via USB and exposes its functionality through a ROS interface.

The dummy payload visible in Fig. 19 features a replaceable top part that can accommodate the printed synthetic shapes of around 40 mm in diameter shown in Table 3. The bottom of the container contains extra weight to bring the total weight of the payload to 210 g.

Since the main purpose of this paper is to demonstrate the applicability of TRIGGER on an aerial platform and not the overall flight control of the resulting aerial manipulator, the flight control task has been simplified in a suitable way. In the laboratory, both the UAV and the payload are precisely localized via a motion-capture system. During the pick-and-place tasks, the UAV is remotely piloted, except for the initial descent to the payload where a robust super twisting controller inspired by [55] was used to provide more accurate position control (≤ 3 cm) compared to what the stock PX4 controller is capable of. The same controller was used throughout the synthetic shapes test. On contact, the xy position controller is disabled as shown in Fig. 20 and consequently, the platform relies on the friction between the gripper and payload to keep its position during the evacuation phase. In all cases, the human pilot activates the gripper on first visual contact with the payload. The activation force is not actively controlled as we leave this for future work.
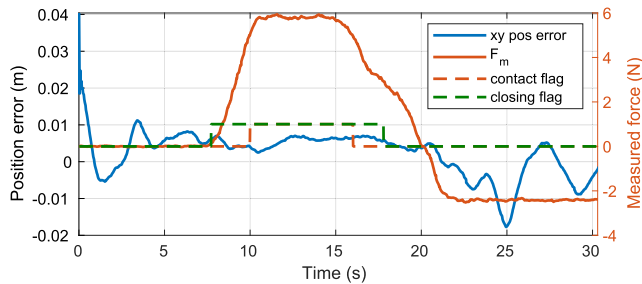
FIGURE 20. To avoid extraneous control action, the xy position controller is disabled on contact as signaled by the contact flag ($F_m \geq 5N$). Driving the roll and pitch angle close to zero and relying on the friction between the payload and the gripper is sufficient to keep the UAV in position while the gripper is closing (indicated by the closing flag). The gripper is activated on first contact by the human pilot.
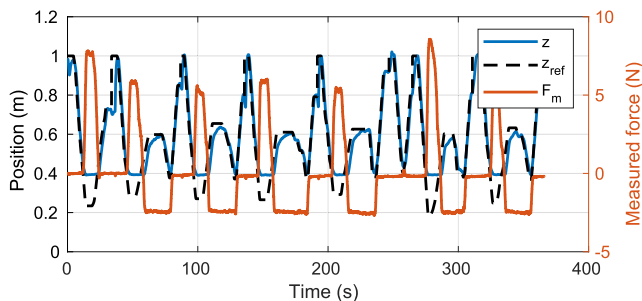
FIGURE 21. Grasp, hold, drop cycles. Altitude z and measured force F_m for multiple repeated grasps. $F_m < 0$ represent holding forces, $F_m > 0$ are contact forces. The first grasp is unsuccessful, the six following grasps are successful as can be seen from the negative F_m values. The payload is held in the air for more than 10s to validate a successful grasp, afterwards it is dropped and picked up again. The grasping attempt at $t = 256s$ was aborted due to a positional error.

To cover a wide range of challenges, a total of 8 synthetic shapes were tested to assess the grasping performance of the aerial platform. Each shape was repeatedly grasped until $\#ge = 6$ grasps with good engagement were obtained (here and in the following, '#' is used in the sense of 'number of'). A typical test series is visualized in Fig. 21. The proper engagement of the gripper was verified visually. If the cargo is held successfully in the air for more than 10 s it is counted as 'held', otherwise it is counted as 'dropped'. It should be noted that a visually good engagement does not imply a successful grasp as the gripper can still fail to produce enough holding force. Cases, where the gripper was unable to engage properly were also counted and labeled as 'discarded'. Those two metrics clearly separate the performance of the gripper represented by *holding chance* = #*held* /#*ge* from the performance of the position controller, resp. the human in the loop defined as *engagement chance* = 1 − (#*discarded* /(#*ge* + #*discarded*))). The product of those two factors yields the total *success chance*.

The experiments were carried out with the sticky 15 % *deadener* and 66 % fill ratio membrane. In total, 66 samples were collected.

B. RESULTS

The pick-and-place experiment is visualized in Fig. 19 for various time instances, where the aerial grasping system

successfully picks up the payload (in blue with the 'cube' shape) and places it on top of the barrel. Aggressive roll maneuvers after picking up the payload verified a solid grasp of the cargo. The UAV both started and landed on the gripper itself. The full pick-and-place experiment is best seen in video.[1]

The results regarding the grasping of the synthetic shapes are given in Table 3. The data shows that the shapes 'cube', 'ridge', 'cake', 'cylinder (hollow)', and 'tube' were able to be held successfully in almost all cases. Those shapes are thus particularly simple to hold as they feature vertical faces. The 'ball' was harder to hold onto as with a diameter of 50 mm, it is on the upper end of what the gripper can reasonably be expected to grasp. It was further observed that only the sticky membrane was able to hold it properly. The 'triangle' was almost impossible to hold with only one successful attempt and one where the cargo was dropped after a few seconds. A possible explanation could be that the limited surface area is not giving the gripper enough material to hold onto. As anticipated, the 'pyramid' shape was impossible to lift due to the squeezing effect that causes the shape to become wedged out of the grasp.
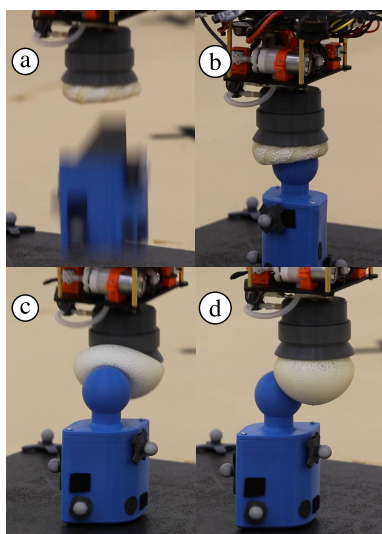
The engagement chance for the 'ridge' and 'pyramid', 'cube', and 'cake' was above 75 %. It was thus easy to get the gripper in a good position to engage properly, where only the narrow edge of the 'cake' was a minor issue. The 'cube, 'cake', 'ridge', 'tube', and 'pyramid' furthermore showed to be self-centering, with the UAV snapping in position of the payload upon closing the gripper. We think this is caused by the taper on the wedge shown in Fig. 4. Curiously, despite the slanted top surface, the 'triangle' was easy to grasp and also exhibited self-centering behavior. The 'ball' shape proved to be very challenging to engage with a chance of only 46.2 %. In most cases, the membrane just slipped off the sides of the sphere unless precisely hit in the center. Unlike stationary robots, the aerial platform is floating and thus even small contact forces in x and y directions can dislocate it significantly from the ideal center position. The 'tube' shares aspects of the 'ball' and 'cube' primitives and therefore performance was in between those two, with only three cases where the gripper slipped before it had the chance to engage properly. The 'hollow cylinder' was also only engaged successfully when hit close to the center and generally slipped off when hitting the narrow outer walls.

The failure modes encountered during the experiment were slippage, positional errors, ill-timed closure of the gripper, and dropping due to a lack of significant holding force. Slippage was observed on shapes where the gripper makes contact with round or slanted edges such as the 'ball', 'tube', and the 'triangle' that dislocated the UAV in xy-plane. It represents the most common failure mode with 43 %, 100 %, and 67 % of all engagement failures for the shapes 'ball', 'hollow cylinder' and 'tube' respectively. Positional errors were sparse thanks to the super-twisting position controller.

---

[1]Supplementary video: https://youtu.be/s5J6Mv4Wp1E

TABLE 3. Experimental results of TRIGGER (15% deadener, 66% fill ratio) grasping different shapes of 210g from a UAV. The overall success chance depends on the shape of the payload. The holding chance benchmarks the performance of the gripper in case of successful engagement. The engagement chance describes other factors (e.g., positional accuracy, human errors) that would prevent the successful mating of the gripper and the payload.

	ball	cube	cylinder (hollow)	cake	triangle	tube	ridge	pyramid
# held/dropped # discarded	4/2 7	6/0 1	6/0 4	6/0 2	1/5 1	5/1 3	6/0 0	0/6 0
holding chance engagement chance	66.7 % 46.2 %	100 % 85.7 %	100 % 60 %	100 % 75 %	16.7 % 85.7 %	83.3 % 66.7 %	100 % 100 %	0 % 100 %
success chance	30.8 %	85.7 %	60 %	75 %	14.3 %	55.6 %	100 %	0 %

FIGURE 22. Possible failure modes: (a) insufficient holding force, (b) lack of penetration depth due to premature closure, (c) slippage, (d) positional error.

However, good positional accuracy is imperative for reliable engagements. Premature closure and/or insufficient descend rate of the gripper can result in the lack of sufficient penetration depth and consequently lack or absence of holding force. Delayed closure of the air-filled membrane is more likely to cause slippage. The failure modes are shown in Fig. 22. Failures due to slippage and positional errors are most likely unique to this application of the UG. Stationary robots exhibit much better positional accuracy and are not easily dislocated by reaction forces.

The total success chance was the highest for 'cube' and 'ridge' with over 85 %, followed by 'cake', 'hollow cylinder', and 'tube' with over 55 %. The most challenging candidates were the 'ball' and the 'triangle' with 30 % resp. 14 %. The 'pyramid' was not expected to be graspable as not even a human hand can hold onto it.

In conclusion, the engagement chance is currently the most limiting factor. Failure modes (c) and (d) (see Fig. 22) are addressable via mechanical changes. A straightforward improvement addressing failure mode (d) consists in extending the size of the membrane, which would increase the gripper's tolerance towards positional errors. Regarding the slippage problem (c) on 'ball' and 'tube' shapes, the bag-shaped membrane has shown to be suboptimal due to the reaction forces it generated in xy-plane. A cup shape could likely be ideal as it would reinforce the self-centering effect observed for some test shapes. Further investigation is thus required as changing the shape of the membrane also impacts the holding force [47] and there might be a tradeoff between having a membrane that engages reliably and having it develop high holding forces. Failure mode (b) can be addressed by proper force control during the evacuation phase of the gripper, taking the human operator out of the loop (left for future work). Failure mode (a) is inherent to certain shapes (e.g., 'triangle' and 'pyramid'). We believe a stronger vacuum could address this problem to a certain degree.

VI. DISCUSSION

The development of soft grippers for aerial vehicles has gained interest due to the advantageous properties of soft materials, which are a natural match for aerial grasping. In contrast to their rigid counterparts, soft grippers are tolerant towards unknown object geometries and surfaces and do not require high positional accuracy for successful grasps. By developing a lightweight soft jamming universal gripper attached to a UAV we further advanced the potential of soft aerial grasping. Compared to available soft grippers for aerial grasping, the developed system exhibits several characteristics that are worth discussing.

The developed gripper is highly integrated and modular and the tight integration of the electronics, software, sensors and mechanics leads to significant weight savings and enables a well-defined grasping procedure that can be automated for use in autonomous systems. The modularity not only helps in iterating the design rapidly, but it also addresses some concerns typically associated with UGs. By having an explicit interface between the grasping part (membrane module) and the supporting hardware, we assure that the membrane is quick and easy (toolless) to swap in case of damage. Other types of pneumatic grippers could also make use of this interface, e.g., suction cups. Thanks to the specific characteristics of our UG's construction, it is particularly

well suited for aerial vehicles, comparable to the typical multi-fingered soft grippers, but with some unique features (e.g., omnidirectionality, or the ability to use as landing gear).

TRIGGER is omnidirectional in contrast to other available soft aerial grasping systems (e.g., claws), which are sensitive to the angle the payload is approached. The same applies to lateral position errors, where the UG tolerates displacements as large as 60 % of its diameter. This relaxes the requirements in terms of necessary grasping accuracy, which is especially advantageous for aerial systems that are subjected to external disturbances (e.g., wind gusts, ground effect) and sensor inaccuracies. The required grasping accuracy is proportional to the relative size of the membrane and the payload. For scenarios where precise position control (≤ 3 cm) is not possible, we recommend a proportionally larger membrane than the $\varnothing 80$ mm shown here. During contact, the UAV retains most of its degrees of freedom due to the gripper's elasticity. As such, it can still rotate (pitch and roll) and therefore preserve hover conditions, but at the same time, the translational degrees of freedom are soft-locked by the friction between the payload and the gripper. This would address one concern associated with soft finger grippers. The authors of [23] stated that during their experiment, the multicopter had to land on the ground due to ground effects and the resulting lack of precise position control. During our aerial experiment, we did not observe such a problem as the UAV passively stayed locked in place during the grasp.

Unlike soft fingers, our UG forms a rigid-like flat surface once a vacuum is established and thus enables the UAV to rest on it. This feature makes our manipulating UAV system exceptional as it removes the need for a dedicated landing gear that also often interferes with the attached gripper resp. the sensors required for autonomous grasping. Moreover, using the UG as landing gear further reduces the weight of the aerial system. The system is also able (within limits) to compensate for some terrain imperfections (e.g., slanted surfaces or small rocks), assuring optimal takeoff and land conditions. Traditional soft finger grippers often cannot prevent the payload from moving after the grasp is established, which can create further disturbances during flight. Contrary to our UG, which forms a system behaving much more akin to a single rigid body due to the jamming of the granular material.

Hard shocks typically associated with the impact of two bodies are problematic both from a mechanical perspective, like the risk of damage, and also from a control perspective (e.g., potential instability). Passive mechanical compliance alleviates this problem by spreading the impact over a larger time interval. The developed UG is completely soft during the first contact phase and is thus passively compliant and absorbs and dampens shocks. This applies to both landing and grasping scenarios.

Our gripper develops 15 N of holding force on our test peg that does not allow for geometric interlocking and thus purely relies on friction and suction (to a much lesser extent), which is, therefore, a worst-case scenario. As indicated in [50],

geometric interlocking can dramatically increase the holding force. Comparisons with other UGs are hard to make due to the lack of a standardized test procedure. However, comparing our results with the work of [43], [50], and [56], it can be said that the measured holding force for objects without geometric interlocking is in the same neighborhood, i.e., 10 N-30 N, while consuming significantly less power (less than 10 W against several hundreds of watts) and operating at a lower pressure differential. This is partially thanks to the adhesion stemming from the deadener. Consequently, also the cycle times of our solution are longer (11 s against 4 s) and have to be handled properly, and failure to do so will result in degraded or even unsuccessful grasps. Therefore, in the larger context of UGs, our results indicate that high-power pumps are not strictly required, but are nevertheless beneficial (faster cycle times and higher hold forces). In practice, fitting larger, heavier pumps is limited by the payload capacity of the aerial platform. Therefore, for applications that benefit from near-instantaneous activation (e.g., perching), magnetically activated jamming [39] could be a good alternative.

The current design limits the gripper to grasp objects solemnly from the floor (claw configuration aside). Two problems arise when grasping from other directions, e.g., horizontally. First, the granular material accumulates along the direction of gravity, which reduces the performance of the gripper as there is no longer an even spread of the material around the grasped object. Second, the object has to be able to withstand a pushing force (i.e., the activation force) without tipping or sliding. We think the former can be addressed by a change in the membrane's design, e.g., a chambered construction that prevents adverse accumulation of the granular material. The latter is inherent to the grasping mechanism, but as shown in Section III, it can be reduced to a fairly small amount (250 gf). Both issues are not present in the claw configuration demonstrated here but could cause problems in conjunction with the bigger configuration space provided by a serial link manipulator.

VII. CONCLUSION

This work introduced TRIGGER, a novel, highly integrated, and lightweight UG with a low activation force requirement for aerial manipulation. We experimentally validated the presented gripper and determined the optimal minimum activation force required to work reliably. We also concluded that the relation between the activation force and the resulting holding force is highly dependent on the fill ratio, i.e., lower fill ratios are preferable since they lower the required activation force. We further investigated possible holding force improvements using a silicone additive (*deadener*), which yielded a 52 % higher holding force compared to the reference case without deadener.

Based on our bench-top experimental data, a simulation model was developed that faithfully represents the most relevant aspects of TRIGGER intended for numerical robotics simulators. A considerable number of aerial grasping
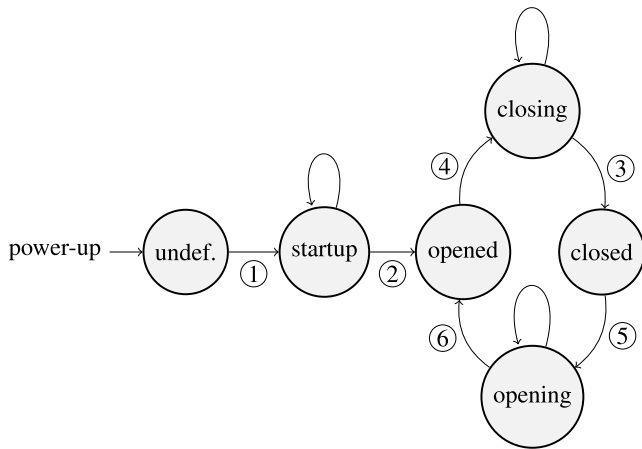
FIGURE 23. Gripper automaton. The gripper's behavior is governed by the state machine, transitioning between states once certain conditions are met. The main states are 'opened' and 'closed' with intermediary states to handle transitions in between. In the beginning, the state of the gripper is not known; therefore, it requires an initial boot procedure. Afterward, the state is well-defined by the data the sensors are providing.

experiments confirmed the gripper's ability to hold objects of a variety of shapes.

Regarding the design, we believe that significant weight savings can still be achieved by having some of the structural components fabricated out of carbon fiber (e.g., the base plate), which would, nonetheless, increase the costs of the solution. Our membrane casting technique allows the creation of internal and external features on the membrane, which could potentially have interesting effects on the behavior of the gripper. The design and the potential effects of those features could be a topic of future work.

As shown by our experiments, the presented gripper benefits from controlling the activation force during the grasping interval as it is key for safe and reliable grasping. Upcoming work thus features the development of a force controller that enables the tracking of the nominal activation force during the time the gripper is closing as well as more experiments. Furthermore, trajectory optimization will be used to guide the UAV to the payload under consideration of the particularities of the UG. These developments aim to automate the aerial grasping process and take the human factor out of the loop.

APPENDIX

Herein the state machine (automaton) as it is depicted in Fig. 23 is described. At the beginning (power-up), we assume the state of the gripper to be undefined as it could be either jammed or fluidized. Thus, we start ① by running a 'startup' cycle which pulls all the air out of the membrane, then refills it until $P > P_{max}$ is reached, then enters the 'opened' state via ② indicating that the gripper is ready for operation. The transitions ③ and ⑥ depend on time and internal pressure. For the closing operation ③ the condition is $P < P_{min}$ or $t > t_{vacc}$. Transition ④ is automatically triggered if $F_m > F_{thr}$ is measured. The opening condition for transition ⑥ is defined as $P > P_{max}$ or $t > t_{infl}$. The time condition is an additional safety feature in case of sensor malfunction. State transition

⑤ is typically triggered via user command over the serial port. During the 'opening' and 'closing' states, one of the two pumps is running, pumping air either in or out of the system.

REFERENCES

[1] J. L. Sanchez-Lopez, M. Molina, H. Bavle, C. Sampedro, R. A. Suárez Fernández, and P. Campoy, "A multi-layered component-based approach for the development of aerial robotic systems: The aerostack framework," *J. Intell. Robot. Syst.*, vol. 88, nos. 2–4, pp. 683–709, Dec. 2017.

[2] J. L. Sanchez-Lopez, R. A. S. Fernández, H. Bavle, C. Sampedro, M. Molina, J. Pestana, and P. Campoy, "AEROSTACK: An architecture and open-source software framework for aerial robotics," in *Proc. Int. Conf. Unmanned Aircr. Syst. (ICUAS)*, Jun. 2016, pp. 332–341.

[3] A. Shukla and H. Karki, "Application of robotics in onshore oil and gas industry—A review. Part I," *Robot. Auto. Syst.*, vol. 75, pp. 490–507, Jan. 2016. [Online]. Available: https://linkinghub.elsevier.com/retrieve/pii/S0921889015002006

[4] D. W. Casbeer, D. B. Kingston, R. W. Beard, and T. W. McLain, "Cooperative forest fire surveillance using a team of small unmanned air vehicles," *Int. J. Syst. Sci.*, vol. 37, no. 6, pp. 351–360, May 2006. [Online]. Available: http://www.tandfonline.com/doi/abs/10.1080/00207720500438480

[5] B. S. Faiçal, F. G. Costa, G. Pessin, J. Ueyama, H. Freitas, A. Colombo, P. H. Fini, L. Villas, F. S. Osório, P. A. Vargas, and T. Braun, "The use of unmanned aerial vehicles and wireless sensor networks for spraying pesticides," *J. Syst. Archit.*, vol. 60, no. 4, pp. 393–404, Apr. 2014. [Online]. Available: https://linkinghub.elsevier.com/retrieve/pii/S1383762114000204

[6] R. W. Beard, T. W. McLain, D. B. Nelson, D. Kingston, and D. Johanson, "Decentralized cooperative aerial surveillance using fixed-wing miniature UAVs," *Proc. IEEE*, vol. 94, no. 7, pp. 1306–1324, Jul. 2006. [Online]. Available: http://ieeexplore.ieee.org/document/1677946/

[7] H. A. Almurib, P. T. Nathan, and T. N. Kumar, "Control and path planning of quadrotor aerial vehicles for search and rescue," in *Proc. SICE Annu. Conf.*, no. 2, 2011, pp. 700–705.

[8] M. T. Connolly, "The use of multi rotor remotely operated aerial vehicles ROAVs as a method of close visually inspecting CVI live and difficult to access assets on offshore platforms," in *Proc. Abu Dhabi Int. Petroleum Exhib. Conf.*, Abu Dhabi, United Arab Emirates, Nov. 2014, pp. 4788–4801. [Online]. Available: https://onepetro.org/SPEADIP/proceedings/14ADIP/1-14ADIP/Abu Dhabi, UAE/210364

[9] H. Li, B. Wang, L. Liu, G. Tian, T. Zheng, and J. Zhang, "The design and application of smartcopter: An unmanned helicopter based robot for transmission line inspection," in *Proc. Chin. Autom. Congr.*, Nov. 2013, pp. 697–702. [Online]. Available: http://ieeexplore.ieee.org/document/6775824/

[10] A. Carrio, J. Pestana, J.-L. Sanchez-Lopez, R. Suarez-Fernandez, P. Campoy, R. Tendero, M. García-De-Viedma, B. González-Rodrigo, J. Bonatti, J. G. Rejas-Ayuga, R. Martínez-Marín, and M. Marchamalo-Sacristán, "UBRISTES: UAV-based building rehabilitation with visible and thermal infrared remote sensing," in *Proc. Robot, 2nd Iberian Robot. Conf.*, L. P. Reis, A. P. Moreira, P. U. Lima, L. Montano, and V. Muñoz-Martinez, Eds. Cham, Switzerland: Springer, 2016, pp. 245–256.

[11] R. A. S. Fernandez, J. L. Sanchez-Lopez, C. Sampedro, H. Bavle, M. Molina, and P. Campoy, "Natural user interfaces for human-drone multi-modal interaction," in *Proc. Int. Conf. Unmanned Aircr. Syst. (ICUAS)*, Jun. 2016, pp. 1013–1022.

[12] H. B. Khamseh, F. Janabi-Sharifi, and A. Abdessameud, "Aerial manipulation—A literature survey," *Robot. Auto. Syst.*, vol. 107, pp. 221–235, Sep. 2018. [Online]. Available: https://linkinghub.elsevier.com/retrieve/pii/S0921889017305535

[13] K. M. Popek, M. S. Johannes, K. C. Wolfe, R. A. Hegeman, J. M. Hatch, J. L. Moore, K. D. Katyal, B. Y. Yeh, and R. J. Bamberger, "Autonomous grasping robotic aerial system for perching (AGRASP)," in *Proc. IEEE/RSJ Int. Conf. Intell. Robots Syst. (IROS)*, Oct. 2018, pp. 1–9. [Online]. Available: https://ieeexplore.ieee.org/document/8593669/

[14] L. Kruse and J. Bradley, "A hybrid, actively compliant manipulator/gripper for aerial manipulation with a multicopter," in *Proc. IEEE Int. Symp. Saf., Secur., Rescue Robot. (SSRR)*, Aug. 2018, pp. 1–8. [Online]. Available: https://ieeexplore.ieee.org/document/8468651/

[15] C. A. Thiels, J. M. Aho, S. P. Zietlow, and D. H. Jenkins, "Use of unmanned aerial vehicles for medical product transport," *Air Med. J.*, vol. 34, no. 2, pp. 104–108, Mar. 2015. [Online]. Available: https://linkinghub.elsevier.com/retrieve/pii/S1067991X14003332

[16] F. J. G. Rubiales, P. Ramon Soria, B. C. Arrue, and A. Ollero, "Soft-tentacle gripper for pipe crawling to inspect industrial facilities using UAVs," *Sensors*, vol. 21, no. 12, p. 4142, Jun. 2021. [Online]. Available: https://www.mdpi.com/1424-8220/21/12/4142

[17] K. Bodie, M. Brunner, M. Pantic, S. Walser, P. Pfndler, U. Angst, R. Siegwart, and J. Nieto, "An omnidirectional aerial manipulation platform for contact-based inspection," in *Proc. Robot., Sci. Syst. XV*. Robotics: Science and Systems Foundation, Jun. 2019, pp. 1–9. [Online]. Available: http://arxiv.org/abs/1905.03502

[18] G. Loianno and V. Kumar, "Cooperative transportation using small quadrotors using monocular vision and inertial sensing," *IEEE Robot. Autom. Lett.*, vol. 3, no. 2, pp. 680–687, Apr. 2018. [Online]. Available: http://ieeexplore.ieee.org/document/8120115/

[19] J.-P. Ore, S. Elbaum, A. Burgin, and C. Detweiler, "Autonomous aerial water sampling," *J. Field Robot.*, vol. 32, no. 8, pp. 1095–1113, Dec. 2015. [Online]. Available: https://onlinelibrary.wiley.com/doi/10.1002/rob.21591

[20] F. Käslin, T. Baur, P. Meier, P. Koller, N. Buchmann, P. D'Odorico, and W. Eugster, "Novel twig sampling method by unmanned aerial vehicle (UAV)," *Frontiers Forests Global Change*, vol. 1, p. 2, Oct. 2018. [Online]. Available: https://www.frontiersin.org/article/10.3389/ffgc.2018.00002/full

[21] C. C. Kessens, J. Thomas, J. P. Desai, and V. Kumar, "Versatile aerial grasping using self-sealing suction," in *Proc. IEEE Int. Conf. Robot. Autom. (ICRA)*, May 2016, pp. 3249–3254. [Online]. Available: http://ieeexplore.ieee.org/document/7487495/

[22] U. A. Fiaz, M. Abdelkader, and J. S. Shamma, "An intelligent gripper design for autonomous aerial transport with passive magnetic grasping and dual-impulsive release," in *Proc. IEEE/ASME Int. Conf. Adv. Intell. Mechatronics (AIM)*, Jul. 2018, pp. 1027–1032. [Online]. Available: https://ieeexplore.ieee.org/document/8452383/

[23] S. Mishra, D. Yang, C. Thalman, P. Polygerinos, and W. Zhang, "Design and control of a hexacopter with soft grasper for autonomous object detection and grasping," in *Proc. Modeling Validation, Multi-Agent Netw. Syst., Path Planning Motion Control, Tracking Control Syst., Unmanned Aerial Vehicles (UAVs) Appl., Unmanned Ground Aerial Vehicles, Vib. Mech. Syst. Vib.*, vol. 3. New York, NY, USA: American Society of Mechanical Engineers, Sep. 2018, Art. no. V003T36A003. [Online]. Available: https://asmedigitalcollection.asme.org/DSCC/proceedings/DSCC2018/51913/Atlanta,Georgia,USA/270951

[24] G. Miron, B. Bédard, and J.-S. Plante, "Sleeved bending actuators for soft grippers: A durable solution for high force-to-weight applications," *Actuators*, vol. 7, no. 3, p. 40, Jul. 2018. [Online]. Available: http://www.mdpi.com/2076-0825/7/3/40

[25] A. McLaren, Z. Fitzgerald, G. Gao, and M. Liarokapis, "A passive closing, tendon driven, adaptive robot hand for ultra-fast, aerial grasping and perching," in *Proc. IEEE/RSJ Int. Conf. Intell. Robots Syst. (IROS)*, Nov. 2019, pp. 5602–5607. [Online]. Available: https://ieeexplore.ieee.org/document/8968076/

[26] M. Lieret, J. Lukas, M. Nikol, and J. Franke, "A lightweight, low-cost and self-diagnosing mechatronic jaw gripper for the aerial picking with unmanned aerial vehicles," *Proc. Manuf.*, vol. 51, pp. 424–430, Jan. 2020. [Online]. Available: https://linkinghub.elsevier.com/retrieve/pii/S2351978920319156

[27] H. Zhang, E. Lerner, B. Cheng, and J. Zhao, "Compliant bistable grippers enable passive perching for micro aerial vehicles," *IEEE/ASME Trans. Mechatronics*, vol. 26, no. 5, pp. 2316–2326, Oct. 2021. [Online]. Available: https://ieeexplore.ieee.org/document/9257095/

[28] H. Tsukagoshi and Y. Osada, "Soft hybrid suction cup capable of sticking to various objects and environments," *Actuators*, vol. 10, no. 3, p. 50, Mar. 2021. [Online]. Available: https://www.mdpi.com/2076-0825/10/3/50

[29] L. Y. Lee, O. A. Syadiqeen, C. P. Tan, and S. G. Nurzaman, "Closed-structure compliant gripper with morphologically optimized multi-material fingertips for aerial grasping," *IEEE Robot. Autom. Lett.*, vol. 6, no. 2, pp. 887–894, Apr. 2021. [Online]. Available: https://ieeexplore.ieee.org/document/9327489/

[30] A. Appius, E. Bauer, M. Blöchlinger, A. Kalra, R. Oberson, A. Raayatsanati, P. Strauch, S. Suresh, M. von Salis, and R. K. Katzschmann, "RAPTOR: Rapid aerial pickup and transport of objects by robots," Mar. 2022, *arXiv:2203.03018*.

[31] D. Tscholl, S.-D. Gravert, A. X. Appius, and R. K. Katzschmann, "Flying hydraulically amplified electrostatic gripper system for aerial object manipulation," May 2022, *arXiv:2205.13011*.

[32] R. R. Ma, L. U. Odhner, and A. M. Dollar, "A modular, open-source 3D printed underactuated hand," in *Proc. IEEE Int. Conf. Robot. Autom.*, May 2013, pp. 2737–2743. [Online]. Available: http://ieeexplore.ieee.org/document/6630954/

[33] S. D'Avella, P. Tripicchio, and C. A. Avizzano, "A study on picking objects in cluttered environments: Exploiting depth features for a custom low-cost universal jamming gripper," *Robot. Comput.-Integr. Manuf.*, vol. 63, Jun. 2020, Art. no. 101888. [Online]. Available: https://linkinghub.elsevier.com/retrieve/pii/S0736584519307276

[34] P. E. Pounds and A. M. Dollar, "Towards grasping with a helicopter platform: Landing accuracy and other challenges," in *Proc. Australas. Conf. Robot. Autom. (ACRA)*, 2010, pp. 1–10.

[35] E. Milana, "Soft robotics for infrastructure protection," *Frontiers Robot. AI*, vol. 9, pp. 1–7, Nov. 2022. [Online]. Available: https://www.frontiersin.org/articles/10.3389/frobt.2022.1026891/full

[36] J. Fishman, S. Ubellacker, N. Hughes, and L. Carlone, "Dynamic grasping with a 'soft' drone: From theory to practice," in *Proc. IEEE/RSJ Int. Conf. Intell. Robots Syst. (IROS)*, Sep. 2021, pp. 4214–4221. [Online]. Available: https://ieeexplore.ieee.org/document/9635927/

[37] E. Brown, N. Rodenberg, J. Amend, A. Mozeika, E. Steltz, M. R. Zakin, H. Lipson, and H. M. Jaeger, "Universal robotic gripper based on the jamming of granular material," *Proc. Nat. Acad. Sci. USA*, vol. 107, no. 44, pp. 18809–18814, Nov. 2010. [Online]. Available: https://pnas.org/doi/full/10.1073/pnas.1003250107

[38] R. P. Behringer and B. Chakraborty, "The physics of jamming for granular materials: A review," *Rep. Prog. Phys.*, vol. 82, no. 1, Jan. 2019, Art. no. 012601. [Online]. Available: https://iopscience.iop.org/article/10.1088/1361-6633/aadc3c

[39] T. Nishida, Y. Okatani, and K. Tadakuma, "Development of universal robot gripper using MR α fluid," *Int. J. Hum. Robot.*, vol. 13, no. 4, Dec. 2016, Art. no. 1650017. [Online]. Available: https://www.worldscientific.com/doi/abs/10.1142/S0219843616500171

[40] T. Sakuma, F. Von Drigalski, M. Ding, J. Takamatsu, and T. Ogasawara, "A universal gripper using optical sensing to acquire tactile information and membrane deformation," in *Proc. IEEE/RSJ Int. Conf. Intell. Robots Syst. (IROS)*, Oct. 2018, pp. 1–9. [Online]. Available: https://ieeexplore.ieee.org/document/8593697

[41] J. R. Amend, E. Brown, N. Rodenberg, H. M. Jaeger, and H. Lipson, "A positive pressure universal gripper based on the jamming of granular material," *IEEE Trans. Robot.*, vol. 28, no. 2, pp. 341–350, Apr. 2012. [Online]. Available: http://ieeexplore.ieee.org/document/6142115/

[42] Y. Wang, Z. Yang, H. Zhou, C. Zhao, B. Barimah, B. Li, C. Xiang, L. Li, X. Gou, and M. Luo, "Inflatable particle-jammed robotic gripper based on integration of positive pressure and partial filling," *Soft Robot.*, vol. 9, no. 2, pp. 309–323, Apr. 2022.

[43] J. M. Gómez-Paccapelo, A. A. Santarossa, H. D. Bustos, and L. A. Pugnaloni, "Effect of the granular material on the maximum holding force of a granular gripper," *Granular Matter*, vol. 23, no. 1, pp. 1–6, Feb. 2021. [Online]. Available: http://link.springer.com/10.1007/s10035-020-01069-z

[44] H. Götz, A. Santarossa, A. Sack, T. Pöschel, and P. Müller, "Soft particles reinforce robotic grippers: Robotic grippers based on granular jamming of soft particles," *Granular Matter*, vol. 24, no. 1, p. 31, Feb. 2022. [Online]. Available: https://link.springer.com/10.1007/s10035-021-01193-4

[45] D. Howard, J. O'Connor, J. Brett, and G. W. Delaney, "Shape, size, and fabrication effects in 3D printed granular jamming grippers," in *Proc. IEEE 4th Int. Conf. Soft Robot. (RoboSoft)*, Apr. 2021, pp. 458–464. [Online]. Available: https://ieeexplore.ieee.org/document/9479438/

[46] D. Howard, J. O'Connor, J. Letchford, T. Joseph, S. Lin, S. Baldwin, and G. Delaney, "A comprehensive dataset of grains for granular jamming in soft robotics: Grip strength and shock absorption," Dec. 2022, *arXiv:2212.06511*.

[47] D. Howard, J. O'Connor, J. Letchford, J. Brett, T. Joseph, S. Lin, D. Furby, and G. W. Delaney, "Getting a grip: In materio evolution of membrane morphology for soft robotic jamming grippers," in *Proc. IEEE 5th Int. Conf. Soft Robot. (RoboSoft)*, Apr. 2022, pp. 531–538. [Online]. Available: https://ieeexplore.ieee.org/document/9762197/

[48] G. D. Howard, J. Brett, J. O'Connor, J. Letchford, and G. W. Delaney, "One-shot 3D-printed multimaterial soft robotic jamming grippers," *Soft Robot.*, vol. 9, no. 3, pp. 497–508, Jun. 2022. [Online]. Available: https://www.liebertpub.com/doi/10.1089/soro.2020.0154

[49] A. Jiang, T. Ranzani, G. Gerboni, L. Lekstutyte, K. Althoefer, P. Dasgupta, and T. Nanayakkara, "Robotic granular jamming: Does the membrane matter?" *Soft Robot.*, vol. 1, no. 3, pp. 192–201, Sep. 2014.

[50] J. Kapadia and M. Yim, "Design and performance of nubbed fluidizing jamming grippers," in *Proc. IEEE Int. Conf. Robot. Autom.*, May 2012, pp. 5301–5306. [Online]. Available: http://ieeexplore.ieee.org/document/6225111/

[51] P. Kremer, J. L. Sanchez-Lopez, and H. Voos, "A hybrid modelling approach for aerial manipulators," *J. Intell. Robot. Syst.*, vol. 105, no. 4, p. 74, Aug. 2022. [Online]. Available: https://link.springer.com/10.1007/s10846-022-01640-1

[52] S. Licht, E. Collins, D. Ballat-Durand, and M. Lopes-Mendes, "Universal jamming grippers for deep-sea manipulation," in *Proc. OCEANS MTS/IEEE Monterey*, Sep. 2016, pp. 1–5. [Online]. Available: https://ieeexplore.ieee.org/document/7761237/

[53] Z. Chen, H. Rahimi Nohooji, and C.-M. Chew, "Development of topology optimized bending-twisting soft finger," *J. Mech. Robot.*, vol. 14, no. 5, pp. 1–23, Oct. 2022. [Online]. Available: https://asmedigitalcollection.asme.org/mechanismsrobotics/article/14/5/051003/1129058/Development-of-Topology-Optimized-Bending-Twisting

[54] H. Zhu, J. Yang, Y. Zhang, X. Feng, and Z. Ma, "Nonlinear dynamic model of air spring with a damper for vehicle ride comfort," *Nonlinear Dyn.*, vol. 89, no. 2, pp. 1545–1568, Jul. 2017. [Online]. Available: http://link.springer.com/10.1007/s11071-017-3535-9

[55] D. M. K. K. V. Rao, H. Habibi, J. L. Sanchez-Lopez, P. P. Menon, C. Edwards, and H. Voos, "Adaptive super-twisting controller design for accurate trajectory tracking performance of unmanned aerial vehicles," Mar. 2023, *arXiv:2303.11770*.

[56] R. Mishra, T. Philips, G. W. Delaney, and D. Howard, "Vibration improves performance in granular jamming grippers," Sep. 2021, *arXiv:2109.10496*.

PAUL KREMER received the Ph.D. degree from the University of Luxembourg, in 2022. He is currently a Postdoctoral Researcher with the Automation & Robotics Research Group (ARG), Interdisciplinary Centre for Security Reliability and Trust (SnT), University of Luxembourg, headed by Prof. Holger Voose. His research interests include robotics, soft robotics, aerial manipulation, and the design and manufacturing of mechatronic systems.

HAMED RAHIMI NOHOOJI (Member, IEEE) received the Ph.D. degree from Curtin University, Australia, in 2018. He was a Research Fellow with the National University of Singapore (NUS) and UCLouvain, Belgium. He is currently a Postdoctoral Research Associate with the University of Luxembourg. His research interests include soft robotics and the development of control systems with applications in robotics. Furthermore, he is a Guest Associate Editor of *Frontiers in Robotics and AI*, a Topical Advisory Panel Member of *Machines*, and a Section Topical Advisory Panel Member of *Sensors*. He has served as a Guest Editor for *Actuators*, *Sensors*, and the *International Journal of Advanced Robotic Systems*.

JOSE LUIS SANCHEZ-LOPEZ (Member, IEEE) received the Ph.D. degree in robotics from the Technical University of Madrid, in 2017. After being a Visiting Researcher with Arizona State University, AZ, USA, and LAAS-CNRS, Toulouse, France. He is currently a Postdoctoral Research Scientist with the Automation & Robotics Research Group (ARG), Interdisciplinary Centre for Security Reliability and Trust (SnT), University of Luxembourg. He is also the Head of the Aerial Robotics Laboratory, SnT. During his 12 years of experience in the field of robotics, the last four as a postdoctoral researcher, he pursued the research goal of providing mobile robots (with a special emphasis on aerial robots) with the highest level of autonomy, making scientific contributions in the fields of (1) perception and situational awareness based on sensor fusion, state estimation, localization and mapping, computer vision, and machine learning; intelligent and cognitive system architectures for multi-agent systems; and trajectory and path planning and control. He has authored more than 55 scientific publications in international journals and conferences related to these fields (Google Scholar citations 1717, H-index: 22, and i10-index: 33) and holds one patent.

HOLGER VOOS (Member, IEEE) received the degree in electrical engineering with Saarland University and the Ph.D. degree in automatic control from the Technical University of Kaiserslautern, Germany, in 2002. From 2000 to 2004, he was with Bodenseewerk Gerätetechnik GmbH, Germany, where he was a Systems Engineer and the Project Manager in research and development in aerospace and robotics. From 2004 to 2010, he was a Professor with the University of Applied Sciences Ravensburg-Weingarten, Germany, where he is currently the Head of the Mobile Robotics Laboratory. Since 2010, he has been a Full Professor with the Interdisciplinary Centre for Security, Reliability and Trust (SnT), University of Luxembourg, and the Head of the SnT Automation and Robotics Research Group. Since 2020, he has been the Course Director of the Interdisciplinary Space Master (ISM), University of Luxembourg, Faculty of Science, Technology and Medicine (FSTM). He is the author or coauthor of more than 250 publications, comprising books, book chapters and journals, and conference papers. His research interests include perception, situational awareness and motion planning and control for autonomous vehicles and robots, and distributed and networked control and automation.

• • •